JCIM JOURNAL OF CHEMICAL INFORMATION AND MODELING

pubs.acs.org/jcim Article

A Relative Binding Free Energy Framework for Structurally Dissimilar Molecules

Hsu-Chun Tsai, Shi Zhang, Tai-Sung Lee, Timothy J. Giese, Charles Lin, James Xu, Yinhui Yi, Darrin M. York,* Abir Ganguly,* and Albert C. Pan*

Cite This: *J. Chem. Inf. Model.* 2026, 66, 1626−1636 Read Online

ACCESS | Metrics & More | Article Recommendations | Supporting Information

ABSTRACT: Relative binding free energy (RBFE) calculations, widely used to predict the potencies of congeneric small molecules binding to a protein receptor, can greatly increase the efficiency of the hit-to-lead and lead optimization stages of the drug discovery process. Traditional RBFE methods, however, cannot be easily applied to small molecules lacking a common core or binding mode, precluding their use in a challenging but crucial component of many drug discovery campaigns. In principle, an absolute binding free energy (ABFE) method can be applied to such molecules, but ABFE often suffers from high computational cost and poor statistical convergence due to the large amount of additional sampling required when compared to RBFE. Here, we introduce core-hopping binding free energy (CBFE) calculations, a computationally efficient framework for the accurate determination of relative binding free energies between small molecules with different cores, leveraging several recently developed techniques such as Alchemical Enhanced Sampling (ACES) with optimized transformation pathways and flexible λ-spacing, as well as λ-dependent Boresch restraints. We benchmark the performance of CBFE across 4 protein systems consisting of 56 small molecules, and find that the results are consistent with RBFE for a congeneric series of ligands and offer considerable improvement in computational cost and precision relative to ABFE results for a series of small molecules with diverse cores and binding modes. All CBFE-related developments are fully implemented in the GPU-accelerated AMBER free energy module (pmemd.cuda) and are available as part of the latest official AMBER release.

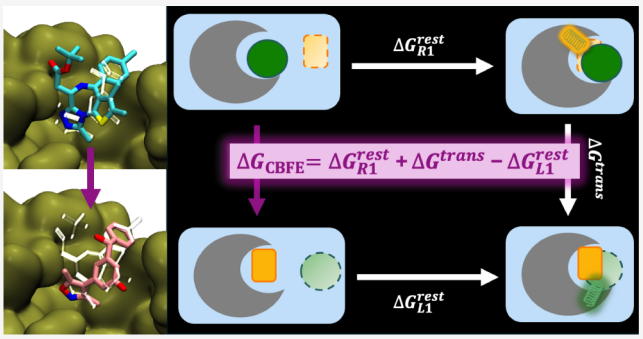

1. INTRODUCTION

Digital potency assays based on binding free energy (BFE) calculations predict how tightly small-molecule ligands bind to proteins at a fraction of the cost and time required for performing the analogous synthesis and assays in the laboratory. In recent years, these calculations have seen large improvements in precision, accuracy, and efficiency due to advances in free energy methods, force fields, software automation, and computational hardware.[1−5]

BFE calculations typically come in two flavors: the more common and widely used form is a relative binding free energy (RBFE) calculation that estimates, often with high precision, the relative binding affinities of two structurally similar ligands binding to a protein. Such calculations are best suited for predicting the relative affinities for a set of congeneric ligands with small R-group modifications and a similar binding mode.[6−8] In such cases, a direct atom mapping can be established between the atoms of the common core shared by the ligands, which improves the phase space overlap between neighboring points along the transformation pathway. These transformations also often involve minimal relaxation of the surrounding environment, thereby reducing the sampling effort required to achieve a given level of precision. By contrast, when ligands lack a common core or binding mode, direct atom mapping is not feasible, and alternative strategies must be employed.

The less common form of BFE calculation is an absolute binding free energy (ABFE) calculation that directly estimates the absolute binding affinities of ligands to their protein targets.[9−11] In theory, ABFE calculations can provide affinity predictions for molecules with completely different scaffolds and binding modes. These calculations, however, are much more involved compared to RBFE calculations, since the free energy of growing the entire ligand in a protein pocket needs to be estimated, including the sampling of conformational changes in and around the protein pocket as the system transitions from an apo to a holo state. In practice, this

Received: September 11, 2025
Revised: January 6, 2026
Accepted: January 9, 2026
Published: January 17, 2026

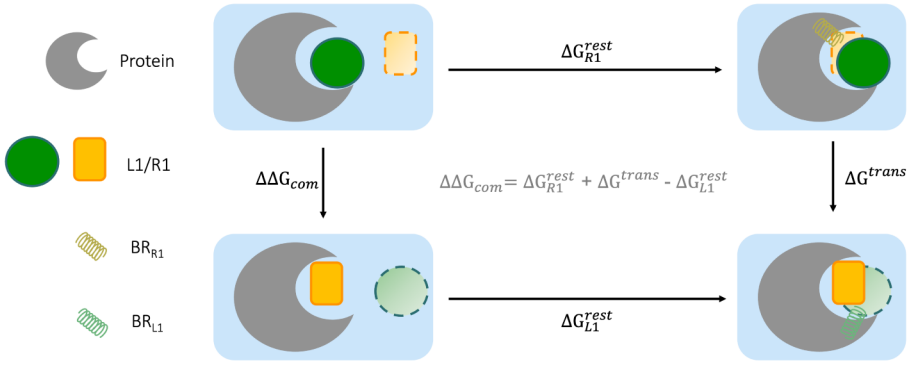

Figure 1. Illustration of the thermodynamic cycle for core-hopping binding free energy calculations. *L*1 (green) and *R*1 (yellow) correspond to the two small molecule ligands undergoing the transformation in the protein (gray) binding site, and BR_{L1} and BR_{L1} correspond to the Boresch restraints acting on *L*1 and *R*1, respectively.

additional sampling often makes ABFE calculations computationally expensive and difficult to converge.

In this work, we present a new approach for determining relative binding affinities, core-hopping binding free energy (CBFE) calculation, that can determine the affinity difference between structurally dissimilar molecules. The CBFE approach leverages two important underlying technologies: the alchemical enhanced sampling (ACES) method[12−14] and λ-dependent Boresch restraints.[9] ACES, described in detail elsewhere[12−14] is an enhanced sampling approach recently integrated into the GPU-accelerated free energy simulation engine in AMBER.[15−17] ACES uses Hamiltonian replica exchange molecular dynamics[18,19] together with an alchemical transformation that leverages a dual-topology framework and several newly developed techniques, including smoothstep softcore potentials for connecting real and enhanced sampling states,[7,20] nonlinear Hamiltonian mixing, and flexible λ scheduling, to achieve efficient enhanced sampling in the alchemical dimension. Recently, we demonstrated the ability of ACES to systematically improve the precision of RBFE calculations across a large and diverse data set of small molecules and protein receptors[13] and developed λ window schedules that optimize phase space overlap and enhance replica-exchange efficiency.[14]

Boresch restraints[9] are harmonic restraints used to restrain the ligand inside the protein binding pocket close to its original pose while in a fully decoupled (noninteracting) state so that this "dummy state"[10] ligand does not leave the pocket. When applied uniformly along the alchemical pathway, these restraints act on both real and decoupled states of the ligand. If chosen in a particular way—typically a set of (at most) 1 distance, two angles, and three dihedrals between the ligand and protein atoms—the net free energy contribution of imposing Boresch restraints to the decoupled state of the ligand can be calculated analytically.[10] Their free energy contribution to the real state of the ligand, though, must be calculated numerically, usually by means of a separate set of simulations.[21−24]

In this work, λ-dependent Boresch restraints (λ-BRs) are introduced that change dynamically along the alchemical λ pathway. Their contributions are absent in the real state and are slowly turned on in concert with other energy terms as the ligand transforms into a decoupled state by smooth elimination of electrostatic and Lennard-Jones interactions with the environment and select internal energy terms to avoid kinetic traps.[20] As the restraints are not present in the real-state end point of the alchemical transformation, they have no contribution to the free energy. The use of λ-BRs, thus obviates the need for performing a separate set of simulations for calculating the free energy contribution of these restraints on the ligand in the real state.

The CBFE approach combines the use of ACES with λ-BRs and thus provides an efficient framework for calculating relative binding free energy differences between two molecules that do not necessarily share a common core within a single set of ACES simulations, making the calculation almost as efficient as RBFE and significantly less expensive than ABFE.

There are few existing approaches for calculating binding free energy differences between noncongeneric molecules.[25−34] Recent methods that have shown considerable promise include the alchemical transfer method (ATM)[25−28] and the separated topologies (SepTop) approach.[29,30] While SepTop is conceptually similar to CBFE, differences lie in their implementation, the form of the alchemical transformation pathway and underlying enhanced sampling methods, as well as the thermodynamic cycles that are used. These are discussed in more detail in the Theory section below.

The remainder of the paper is organized as follows. Section 2 discusses the CBFE framework and the underlying methods, highlighting some of the similarities and differences with other approaches. Section 3 details the computational methods used for system preparation, simulation, and analysis. Section 4 evaluates the CBFE method on a diverse data set and compares its performance against RBFE and ABFE, where applicable. Finally, Section 5 concludes with a summary of key results and main take-home messages from this work.

2. THEORY

2.1. The Core Hopping Binding Free Energy (CBFE) Approach

A CBFE calculation is a relative binding free energy calculation executed as a counterpoised set of ABFE calculations performed concurrently so as to minimize the relaxation of the environment around the ligand; e.g., rearrangement of the binding pocket when a ligand fully disappears. The free energy of binding, $\Delta\Delta G^{\mathrm{CBFE}}$, between two ligands, *L*1 and R1 can be calculated via CBFE as follows:

$$\Delta\Delta G^{\mathrm{CBFE}} = \Delta\Delta G_{\mathrm{com}}^{\mathrm{CBFE}} - \Delta\Delta G_{\mathrm{sol}}^{\mathrm{CBFE}} \quad (1)$$

https://doi.org/10.1021/acs.jcim.5c02204
J. Chem. Inf. Model. 2026, 66, 1626−1636

where, $\Delta\Delta G_{com}^{CBFE}$ and $\Delta\Delta G_{sol}^{CBFE}$ are the free energy changes associated with transforming $L1$ to $R1$ in the protein-bound state and in solution, respectively.

Unlike traditional RBFE, in which the two participating molecules are expected to share a common structural core and the transformation involves alchemically mutating only a small portion of the molecule, CBFE does not require the presence of a shared molecular scaffold; no atom map is needed between $L1$ and $R1$. The approach involves simultaneously annihilating one small molecule while growing another in its place.

The free energy change associated with transforming $L1$ to $R1$ in the protein−ligand complex state, $\Delta\Delta G_{com}^{CBFE}$, is calculated according to eq 2, and involves 3 steps as illustrated in the thermodynamic cycle shown in Figure 1. Steps 1 and 3 involve imposing Boresch restraints[9,10] to the decoupled (noninteracting) states of $R1$ and $L1$, respectively. Here, two different sets of Boresch restraints, BR_{R1} and BR_{L1}, are considered that are specific to the two ligands. Given the special properties of Boresch restraints mentioned earlier, ΔG_{R1}^{Rest} and ΔG_{L1}^{Rest} can be calculated analytically. $\Delta\Delta G_{sol}$ is calculated by performing two absolute solvation free energy (ASFE) calculations for $L1$ and $R1$, independently, as per eq 3.

$$\Delta\Delta G_{com} = \Delta G_{R1}^{rest} + \Delta G^{trans} - \Delta G_{L1}^{rest} \quad (2)$$

$$\Delta\Delta G_{sol} = \Delta G_{R1}^{ASFE} - \Delta G_{L1}^{ASFE} \quad (3)$$

Thus, the key step in CBFE is calculating ΔG^{trans}, which involves transforming $L1$ from its real (fully interacting) state to its noninteracting state held by BR_{L1} and simultaneously converting $R1$ from its noninteracting state held by BR_{R1} to its real state, all within a single ACES Hamiltonian replica exchange MD simulation for a series of λ windows along the alchemical pathway. This concerted transformation is primarily made possible by combining two recently introduced technologies in the AMBER GPU alchemical free energy code.[35] The first, the ACES approach[12] leverages a dual-topology framework to connect end states through robust transformation pathways using smoothstep softcore potentials and nonlinear λ-scheduling. ACES addresses two critical aspects of the calculation: (1) ensuring phase-space overlap between the fully decoupled and real states of the ligand by enabling enhanced sampling and accurate free energy estimates, and (2) improving the stability of alchemical transformations by allowing for large perturbations to be performed effectively and robustly within the alchemical free energy framework.

The second enabling technology involves λ-dependent Boresch restraints. First introduced in Boresch et al.[9] standard Boresch restraints are typically used to maintain the ligand position and orientation in the protein pocket in its decoupled (noninteracting) state. The restraints involve 1 distance, 2 angles, and 3 dihedrals formed between 3 atoms each from the ligand and protein (Figure S1). The notable advantage of using Boresch-style restraints lies in the analytical solution to their free energy contribution to the ligand decoupled state, given by the equation:

$$\Delta G = -k_B T \ln\left[\frac{8\pi^2 V^0 (K_r K_{\theta A} K_{\theta B} K_{\phi A} K_{\phi B} K_{\phi C})^{1/2}}{r_0^2 \sin\theta_{A,0} \sin\theta_{B,0} (2\pi k_B T)^3}\right] \quad (4)$$

where V^0 is the volume corresponding to the one molar standard state (1660 Å^3); r_0 is the reference distance for the restraints; θ_A and θ_B are the reference angles for the restraints; K is the force constant for the distance (r_0), two angles (θ_A and θ_B) and three dihedrals (ϕ_A, ϕ_B, ϕ_C) restraints we applied.

Recently, in the AMBER GPU code, we implemented λ-dependent restraints that linearly scale the force constants such that they can be either gradually grown or removed as a function of λ values. In the ΔG^{trans} step in CBFE, we employ these λ-dependent restraints to construct the Boresch restraints, BR_{L1} and BR_{R1}. The initial ($\lambda = 0$) state of this calculation consists of $L1$ in a real state and $R1$ in a decoupled state, held in the pocket by BR_{R1}. Along the λ windows, as $L1$ is gradually transformed to a decoupled state and $R1$ to a real state, BR_{L1} is grown and simultaneously BR_{R1} is removed, such that in the final ($\lambda = 1$) state, where $R1$ is in real state, BR_{R1} is entirely absent, and $L1$, which is in decoupled state, is held by the fully acting BR_{L1}. Since the restraints are never enforced on the real states of either ligand, a separate calculation for estimating the free energy contribution of these restraints to the ligand real states is not needed.

As noted earlier, two existing approaches for computing relative binding free energies between noncongeneric molecules are ATM[25−28] and SepTop.[29,30] ATM computes the relative binding free energy between two ligands by placing one ligand in the protein and the other in solvent, and then alchemically swapping their coordinates. This avoids the need for dual or hybrid topologies and the partitioning of ligands into common and softcore regions, making the approach applicable to both congeneric and dissimilar compounds and more straightforward to implement in existing molecular dynamics engines. Larger box sizes, however, may be required to accommodate the additional ligand in the bulk solvent. SepTop is conceptually closer to CBFE, but differs in key aspects of implementation. Like CBFE, SepTop involves running two ABFE calculations in opposite directions. While CBFE takes a concerted approach in which the entire ligand transformation occurs within a single HREMD simulation, SepTop, however, adopts a more stepwise protocol in which each ligand is decoupled by first turning off the electrostatics on the full restrained ligand, followed by the van der Waals interactions. The release of restraints from the fully interacting ligand is paired with the van der Waals decoupling step. The concerted alchemical pathway adopted by ACES is made possible by the introduction of the λ-dependent Boresch restraints within the ACES framework. Like ATM and SepTop, CBFE is freely available for academic use as it has been incorporated into the latest version of AMBER.

3. METHODS

Herein, we describe the data sets examined, and computational details used, in the simulations and analysis. The Supporting Information contains details about the structure of each set of ligands, and tabulates specific alchemical transformations conducted for each set of ligands, as well as quantitative values for the predicted binding ΔG, statistical error estimates, and analysis of cycle closure errors.

3.1. Data Sets

In this study, we consider a diverse data set consisting of 56 ligands across 4 protein targets, carefully chosen to assess the accuracy and precision of CBFE on a broad range of molecular transformations that are commonly encountered in drug discovery campaigns. The data set consists of four targets: Tyrosine Kinase 2 (TYK2) drawn from the well-known JACS data set[6] which consists of a series of neutral, congeneric ligands; the checkpoint kinase 1 (CHK1) protein with 5 ligands that exhibit different forms of ring opening/closing/expansion,[36] three different scaffold series of β-secretase 1

https://doi.org/10.1021/acs.jcim.5c02204
J. Chem. Inf. Model. 2026, 66, 1626−1636

(BACE1),[37−39] and the Bromodomain-containing protein 4 (BRD4) with 17 ligands comprising 15 structurally different scaffolds.[40,41] PDB IDs associated with these systems are summarized in Table S1.

3.2. System Preparation and General Simulation Details

The preparation of protein−ligand complexes for all CBFE calculations involved multiple steps utilizing various programs available as part of AmberTools.[42] The *pdb4amber* utility was used to clean the PDB structures, while *tleap* was employed to generate topology and parameter files. In some cases, protonation states of specific titratable residues in the active site were manually assigned based on visual inspection. For target ligands lacking cocrystal structures, 3D poses were generated using a maximum common substructure (MCS) constrained 3D alignment approach, with an existing cocrystal ligand serving as the reference. Protein−ligand complexes and isolated ligands were immersed in separate truncated octahedral boxes of TIP3P waters[43] with buffer distances of 10 and 18 Å, respectively. The protein systems were modeled using the AMBER ff14SB force field[44] while the ligands were parametrized using the General AMBER Force Field (GAFF)[45] with AM1-BCC as the charge model.[46] The Monte Carlo barostat and Langevin thermostat[47] with a friction constant of 2.0 ps^{-1} were used to maintain constant temperature and pressure, respectively. SHAKE[48,49] and Hydrogen Mass Repartitioning (HMR)[50] were applied to both protein−ligand complexes and ligand topologies. Nonbonded interactions were computed directly within an 8 Å cutoff, and long-range electrostatic interactions were evaluated with the particle mesh Ewald (PME) method[51,52] using approximately a 1 Å grid spacing. A 4 fs time step was employed for all simulations, which were performed using the PMEMD.cuda program that is available as part of the official AMBER24 release.[53,54]

3.3. Details Related to CBFE Calculations

Each system was subjected to a rigorous equilibration protocol that has been detailed earlier and briefly summarized here. Each system was first minimized, then gradually heated from 0 to 298 K through a series of alternating short (2 ps) simulations in constant NVT and NPT ensembles, with positional restraints on all protein and ligand heavy atoms. Once equilibrated with restraints, an additional 5 ns NPT molecular dynamics simulation was performed without restraints. Structures at the end of the equilibration stage were used to create the hybrid dual topologies necessary for the CBFE calculations. The complex leg simulations, specifically the calculation of ΔG^{trans} in Figure 1, were performed with 40 equally spaced λ windows, while the solution leg simulations, those related to the ASFE calculations of the ligands, were performed with 40 equally spaced λ windows. The CBFE simulation setup described above was done with an automated, in-house workflow developed at TandemAI.

The initial structures for the different λ windows were obtained using a fast sequential equilibration protocol in which, starting from $\lambda = 0$, each λ is first minimized, heated to 300 K in 60 ps at constant NVT, and then equilibrated at constant NPT for another 60 ps. The structure at the end of this protocol is used as the input structure for the following λ window. This sequential protocol was chosen over the more conventional scheme in which all λ windows are initialized from a common starting structure and equilibrated in parallel, as it typically resulted in more stable simulations. In the parallel approach, instabilities can arise particularly at higher λ values, where the change in Hamiltonian is more significant. In contrast, the sequential protocol ensures that each λ window is initiated from the equilibrated structure of the preceding window, keeping the Hamiltonian change at each λ minimal.

After all λ windows are equilibrated, production runs of 5 ns were carried out in the NVT ensemble. All runs were performed with ACES that uses the HREMD framework within the one-step concerted protocol[55] and modified SSC(2) softcore potentials[20] ($m = n = 2$, $\alpha^{LJ} = 0.5$, $\alpha^{Coul} = 1$). Replica exchanges were attempted every 500 fs. The ACES method uses the dual-topology framework in AMBER and separates the transforming region into a "common core" set of atoms that share coordinates and a set of "softcore" atoms that have separable coordinates. Enhanced sampling is achieved by creation and annihilation of the softcore atoms of the end states and connecting these states with the HREMD network. In CBFE, since one ligand is fully annihilated while the other is grown, the two participating ligands are assigned entirely to the softcore region. Each CBFE calculation was performed in the forward and reverse directions, and repeated 3 times to ensure reproducibility.

We employed Boresch-style protein−ligand restraints to confine the ligand within the protein binding site and prevent its uncontrolled exploration of the simulation box during the decoupling of protein−ligand interactions. These restraints act on three atoms in the protein and three atoms in the ligand through one distance, two angle, and three dihedral restraints, as detailed by Boresch et al.[9] Although the binding free energy is formally independent of the chosen restraint atoms, the selection can influence the convergence and stability of the simulations. Several strategies have therefore been explored to identify protein and ligand atoms that yield robust Boresch restraints.[29,56,57]

Here, we employ a procedure (Figure S1) similar to that described in Huggins et al.[56] with minor modifications. Starting from the equilibrated protein−ligand complex, we first identify the ligand heavy atom a that lies closest to a protein Cα atom, A. This pair of atoms serves as the primary anchor and defines the distance restraint r_{aA} in Figure S1. The second ligand anchor atom b is chosen as a heavy atom within two bonds of a that yields a $b-a-A$ angle closest to 90°. The third ligand anchor atom c is selected as a heavy atom within two bonds of both a and b that produces a $c-b-a$ angle closest to 90°. On the protein side, anchor atoms B and C are taken as the Cα atoms of the residues immediately adjacent to the residue containing atom A. In our internal benchmarks, this procedure consistently produced stable Boresch restraints that preserved the ligand binding-mode orientation in the decoupled state.

3.4. Details Related to RBFE and ABFE Calculations

The RBFE and ABFE calculations performed in this work were carried out using in-house (TandemAI) workflows. The RBFE protocol has been described in detail in an earlier work;[13] here, we briefly summarize the ABFE protocol. The absolute binding free energy of a ligand binding to a protein target, ΔG^{ABFE} is calculated as per eq 5, based on the thermodynamic cycle shown in Figure S2.

$$\Delta G^{ABFE} = \Delta G_{sol}^{decoup} - \Delta G_{com}^{decoup} - \Delta G_{real}^{rest} - \Delta G_{dum}^{rest} \quad (5)$$

where ΔG_{sol}^{decoup} is the free energy associated with decoupling the ligand in solution; ΔG_{com}^{decoup} is the free energy associated with decoupling the ligand, held by Boresch restraints to the protein, in the complex state; ΔG_{real}^{rest} is the free energy associated with imposing Boresch restraints on the ligand in the protein-bound state, and ΔG_{dum}^{rest} is the free energy associated with imposing Boresch restraints on the ligand decoupled state.

System preparation, equilibration protocol and free energy simulation parameters used for ABFE calculations are analogous to those used for CBFE calculations. Simulations for computing ΔG_{sol}^{decoup}, ΔG_{com}^{decoup}, and ΔG_{real}^{rest} were run with 40 λ windows, were run with 40 λ windows, uniformly distributed between 0 and 1. ΔG_{dum}^{rest} was calculated analytically using eq 4. Each ABFE calculation was repeated 3 times to ensure reproducibility.

3.5. Free Energy Analysis

The program FE-ToolKit[58] available as part of the latest version of AmberTools[42,59] was used to analyze the various free energy simulations and calculate ΔGs using the Multistate Bennett's Acceptance Ratio (MBAR) method[60] with cycle-closure corrections based on network-wide free energy analysis[61] in case of CBFE and RBFE. Errors of calculated free energy estimates with respect to experiment are reported as mean unsigned error (MUE) and root mean squared error (RMSE). Statistical uncertainties of calculated free energy values arise from the analyzed time-series data, independent trials, and forward and reverse (hysteresis) runs, and are all integrated into the standard error estimates.

https://doi.org/10.1021/acs.jcim.5c02204
J. Chem. Inf. Model. 2026, 66, 1626−1636

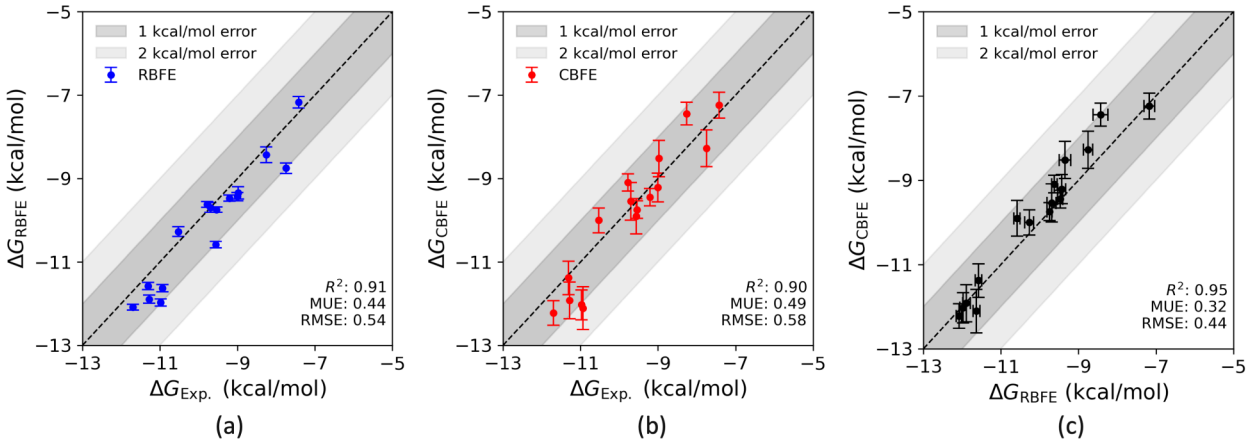

Figure 2. Correlation plots of (a) the experimental values and RBFE results, (b) the experimental values and CBFE results, and (c) the RBFE and CBFE results for TYK2, involving 16 ligands.

In addition, for RBFE and CBFE calculations, an analysis of cycle closure errors within the thermodynamic graph network was conducted. As free energy is a state function, the relative free energy between two nodes in a thermodynamic graph is theoretically independent of the pathway taken to connect the points. As a consequence, any thermodynamic cycle in the graph that begins and ends at the same node (i.e., that "closes" the cycle) should be identically zero. Since the edges of the graph arise from completely independent ACES enhanced sampling simulations, however, these "cycle closure conditions" are not always strictly obeyed and, in some cases, they can deviate significantly from zero. While the network-wide free energy analysis in FE-ToolKit[58] variationally solves the MBAR equations under a set of constraints that all cycle closure conditions are strictly obeyed, it is nonetheless instructive to analyze the unconstrained MBAR edge free energy values for all "minimal" cycles in the network. Here, "minimal cycles" are defined as all minimal-length cycles that cannot be represented as linear combinations of other cycles. The cycle closure errors (CC errors) provide complementary information to the normal statistical errors mentioned above. These standard error estimates consider the variances derived from sampling that have occurred in the simulations. If important regions of phase space are insufficiently sampled or not visited at all, however, then standard error estimates may appear misleadingly small. Analysis of CC errors thus provides additional information about sampling errors that may occur in the network. In some cases, network-wide free energy analysis can flag edges that are potentially problematic. One metric that has been useful in this regard is called a "Lagrange multiplier index" (LMI).[58,61] The LMI for an edge reports the sensitivity of the variational network-wide MBAR procedure to constraining the relative free energy value of two nodes to that of the unconstrained edge value. A large LMI may indicate a problematic edge in the network. If the thermodynamic graph has sufficient redundancy, potentially problematic edges can be eliminated, and the graph reanalyzed. This will lead to new LMI values for the remaining edges. In this way, LMIs can be used iteratively to "prune" the thermodynamic graph in a post-simulation processing step.

4. RESULTS AND DISCUSSION

In this study, we assess the predictive accuracy and precision of the CBFE approach through a series of case studies, utilizing diverse small-molecule data sets that reflect scenarios commonly encountered in real-world drug discovery campaigns. Case study 1 involves a well-studied TYK2 protein–ligand data set consisting of a series of 16 congeneric ligands that share a common molecular scaffold and differ in relatively small changes at a single R-group. Case study 2 focuses on 5 ligands binding to checkpoint kinase 1 (CHK1) that are congeneric, but exhibit large perturbations involving ring formation and expansion. Such changes are known to be challenging for traditional RBFE calculations. Case study 3 focuses on a set of 18 binders to the BACE1 protein that contain 3 different scaffold series, each consisting of 6 ligands. Finally, case study 4 includes 17 structurally diverse small-molecule binders to bromodomain-containing protein 4 (BRD4). Case studies 3 to 4 are typically beyond the scope of traditional RBFE, and accessible only by ABFE calculations. The following sections summarize the CBFE results for these case studies and provide comparisons with existing methods, particularly RBFE and ABFE, where applicable. For each data set (summarized in Table S1), a complete list of calculated free energy values and standard errors are provided in Tables S2–S5 of the Supporting Information, in addition to an extensive discussion of cycle closure errors (Tables S6–S8). In case of the CBFE and ABFE calculations, the analytical solutions to the free energy contributions of the Boresch restraints applied to the ligand decoupled states, ΔG_{R1}^{Rest} and ΔG_{L1}^{Rest} in Figure 1, are not reported separately. However, their absolute values consistently fall within approximately −7 to −8 kcal/mol across all calculations.

4.1. Case Study 1: Application of CBFE to a Congeneric Set of TYK2 Binders

The TYK2 data set represents a system that has been extensively explored by alchemical free energy methods and for which RBFE has been shown to be highly predictive; in a recent study[13] we computed binding free energies for this data set using RBFE and achieved a Pearson correlation (R^2) of 0.91 and mean absolute error (MAE) of 0.44, with experimental data (Figure 2a). Here, we include this data set as a control to ensure that the CBFE results align closely to those from RBFE. In theory, the binding affinity predictions from CBFE and RBFE should be identical. Figure 2 compares the ligand binding free energies of this data set computed using RBFE (Figure 2a) and CBFE (Figure 2b) to the experimental data. In both cases the R^2 is 0.9 and mean unsigned error (MUE) is below 0.5 kcal/mol. This result is significant because the CBFE approach, while expected to afford identical binding free energies as RBFE in theory, follows a fundamentally different protocol. As outlined in the Methods section, RBFE focuses on transforming only the differing R-groups between two ligands while preserving their common core. In contrast,

https://doi.org/10.1021/acs.jcim.5c02204
J. Chem. Inf. Model. 2026, 66, 1626−1636

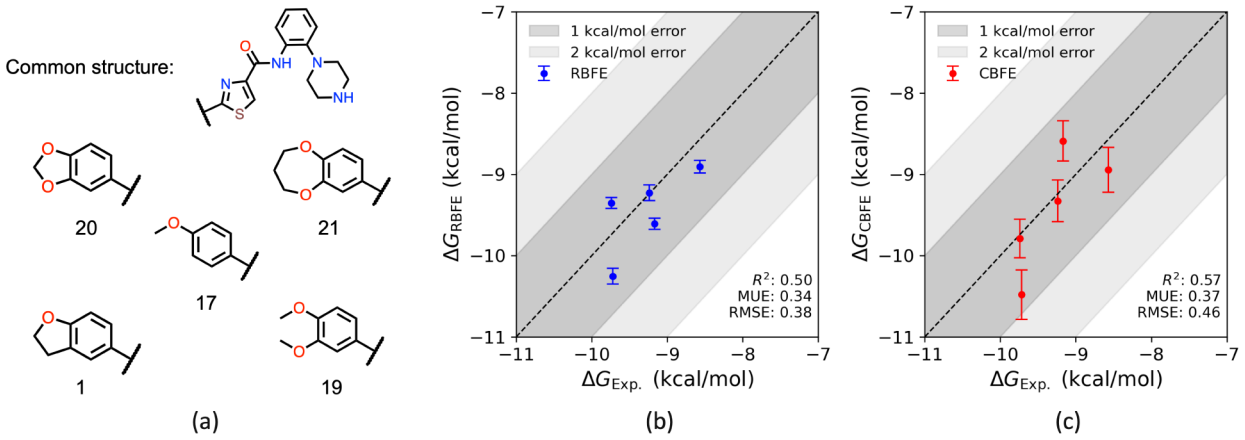

Figure 3. (a) The 2D structures of the **5** CHK1[36] ligands involving a mixture of all types of perturbations, including the regular R-group modification, ring size change perturbation, ring opening/closing perturbation, and ring extension perturbation. (b) Correlation plot of experimental binding free energy values and the prediction values from RBFE for CHK1.[36] (c) Correlation plot of experimental binding free energy values and the prediction values from CBFE for CHK1.[36]

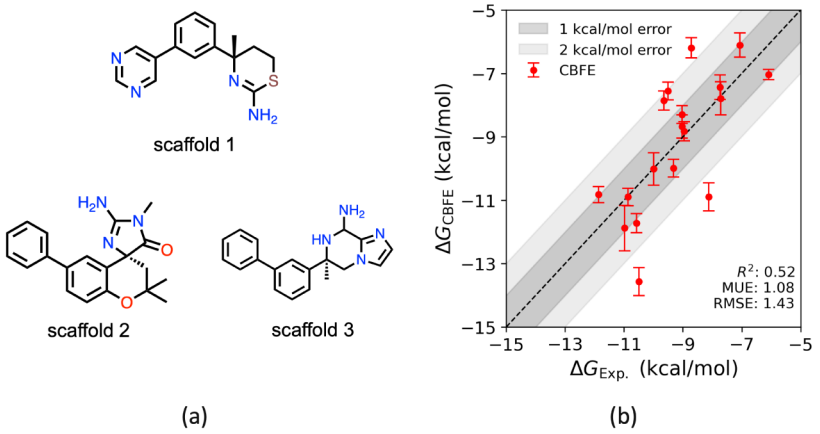

Figure 4. (a) The 2D structures of **3** different scaffolds. (b) Correlation plot of experimental and CBFE binding free energy values for BACE1.[37−39]

CBFE does not rely on shared substructures; instead, one ligand is entirely annihilated to a decoupled state as the other is created from a dummy state. The near-unity correlation (R^2 = 0.95) and low MAE (MAE = 0.32) between the results from these two different approaches (Figure 2c) suggest that CBFE is essentially able to reproduce the RBFE results for this data set.

The larger standard errors estimated for CBFE are not surprising given the much larger perturbations performed in CBFE relative to RBFE. Additionally, cycle-closure (CC) error analysis was conducted to assess the internal consistency of the computed free energy differences within the perturbation network.[61] Interestingly, the mean CC error for the RBFE calculations (0.64 kcal/mol) was higher than that observed for CBFE (0.39 kcal/mol), despite the fact that the standard errors are smaller for RBFE. Indeed, the range of CC errors in RBFE was 0.71−1.51 kcal/mol compared to 0.11−0.96 kcal/mol for CBFE (Table S6).

We suspect that the smaller CC errors in CBFE reflect the differences in how ligand transformations are handled in these two protocols. In RBFE, a shared ligand substructure, the common core, is mapped across an edge and adopts the same coordinates in state A and state B, while atoms attached to the common core are morphed from one moiety to another as part of the softcore region. This use of a common core may restrict the conformational sampling available to the ligand as it morphs from A to B, especially if changes in the softcore region alter the conformational ensemble of the common core atoms in the end states, leading to a cycle closure mismatch. In contrast, a more complete sampling of states A and B is potentially afforded by CBFE because the entire ligand is placed in the softcore region and could explain the reduced CC errors in CBFE.

4.2. Case Study 2: Application of CBFE to a Data Set with Large Perturbations in Ring Topologies

It is well established that traditional RBFE calculations struggle with large alchemical transformations, especially those involving complex structural changes such as ring closure, opening, or expansion, as seen in the CHK1 data set summarized in Figure 3a. For this challenging data set, we compared the performance of CBFE against traditional RBFE. As with the TYK2 ligands, the predicted ΔG values are quite close to the experimental values for RBFE and CBFE (MUE of 0.34 and 0.37 kcal/mol, respectively), with CBFE having larger standard error estimates for the reasons described previously for the TYK2 ligands. Despite the larger standard error estimates, the CBFE values have slightly improved correlation with the experimental values (0.57 versus 0.50 for CBFE and RBFE, respectively). The mean CC error in this system is quite low (0.2 kcal/mol) for both RBFE and CBFE (Table S6),

https://doi.org/10.1021/acs.jcim.5c02204
J. Chem. Inf. Model. 2026, 66, 1626−1636

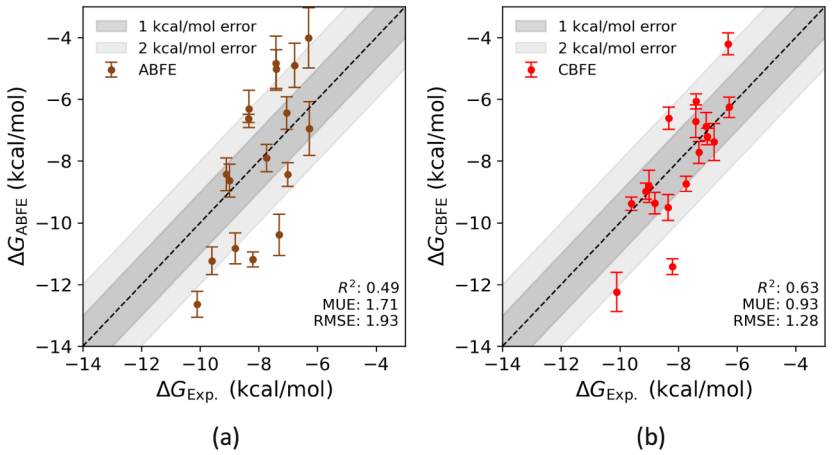

Figure 5. Correlation plot of calculated and experimental binding free energy values for BRD4.[40,41]

suggesting that in both cases similar conformational ensembles are sampled for the ligands in the different transformations in the network.

4.3. Case Study 3: Application of CBFE to a Data Set Containing 3 Different Scaffolds

In case study 3, we focus on 18 binders to BACE1 that span 3 different molecular scaffolds (6 ligands within each scaffold). The different scaffold series are summarized in Figure 4a. We applied CBFE on this data set, with the results summarized in Figure 4b. The correlation between computed binding free energies and experimental values for the BACE1 ligand set demonstrates a reasonable level of predictive accuracy, with R^2 = 0.52. The MUE of 1.08 kcal/mol and RMSE of 1.43 kcal/mol fall within the 2 kcal/mol range often considered acceptable for binding free energy calculations, particularly in challenging systems such as BACE1 inhibitors. Only three ligands have errors in excess of 2 kcal/mol: ligands 5, 11, and 69. The mean cycle closure error for this system is slightly above 1 kcal/mol (Table S6). Given the complexity of the network, which consists of 34 unique cycles formed among the 18 ligands, this result is consistent with the earlier case studies and suggest that CBFE provides more exhaustive sampling of ligand conformational space, thereby yielding comparable conformational ensembles across distinct transformations involving the same ligand. Taken together, these results indicate that the approach provides qualitatively useful estimates of binding affinity while leaving room for methodological improvements to better account for systematic errors and outlier behavior.

4.4. Case Study 4: Application of CBFE to a Data Set Containing Ligands with Multiple Distinct Scaffolds

Case Study 4 focuses on the well-known BRD4 data set, which has previously been used to validate ABFE methods.[62] This data set includes 17 structurally diverse ligands spanning 15 distinct scaffolds, making it unsuitable for traditional RBFE calculations. We independently applied both CBFE and ABFE to this data set, with the results summarized in Figure 5a and b, respectively. Ligand ΔG values calculated using CBFE show slightly better correlation compared to ABFE (R^2 for CBFE = 0.63, R^2 for ABFE = 0.49), as well as improved accuracy, having a lower MUE for CBFE (0.93 kcal/mol) compared to ABFE (1.71 kcal/mol). Whereas 8 ligands have errors exceeding 2 kcal/mol for the ABFE calculations, only 3 ligands have errors in this range with CBFE. Moreover, the standard error estimates of the CBFE ΔG values (range 0.21−0.63 kcal/mol) are markedly narrower than the corresponding ABFE values (range 0.13−0.97 kcal/mol). The mean value of the CC errors for the BRD4 transformations is 0.56 kcal/mol (Table S6). This illustrates that the CBFE approach can reach high precision (on the order of 0.5 kcal/mol) for predicted ΔG values for this challenging system.

4.5. Network-Wide Free Energy Analysis, Lagrange Multiplier Indices, and Cycle Closure Errors

Here, we examine cycle closure (CC) errors derived from the thermodynamic maps used in the RBFE and CBFE calculations and compare the CC error/edge to the range of standard errors derived for each ligand. Detailed error analyses are provided in Tables S2−S8 of the Supporting Information, along with an extended discussion. The CC error analysis for all data sets is presented in Table S6, with additional LMI-based pruning results shown for BACE1 and BRD4 in Tables S7 and S8. Minimal cycles contain 3−5 edges and, while CC errors vary by cycle length, the graphs are too small to draw general trends; CC errors/edge are nevertheless reported for completeness.

For the Tyk2 ligands, RBFE and CBFE show modest CC errors/edge (0.145 and 0.089 kcal/mol). The largest CC errors come from 5-edge cycles, but 3-edge cycles have the largest CC error/edge. CBFE yields smaller CC errors overall, consistent with its more flexible treatment of ligand transformations compared to RBFE as discussed earlier. For the CHK1 system, the RBFE and CBFE exhibit small, comparable CC errors/edge (0.08−0.09 kcal/mol), consistent with their standard error ranges. Precision is generally good for both protocols.

For the BACE1 and BRD4 systems, the CC errors are larger. The BACE1 ligands exhibit a mean CC error of 1.08 kcal/mol, with a maximum CC error of 4.67 kcal/mol, indicating problematic edges in the large, cycle-rich thermodynamic graph. Iterative removal of edges with the highest LMI values significantly reduces CC errors and CC errors/edge, bringing them within the range of per-edge standard errors. However, free energy accuracy (MUE, RMSE) remains largely unchanged, indicating the robustness of the network-wide estimates despite CC error reductions. For the BRD4 system, LMI-based pruning similarly reduces CC errors, CC errors/edge, and their standard deviations across iterations. As with

https://doi.org/10.1021/acs.jcim.5c02204
J. Chem. Inf. Model. 2026, 66, 1626−1636

BACE1, these reductions do not meaningfully change MUE or RMSE relative to experiment.

Overall, for the cases analyzed here, the CC errors can be reduced through LMI-guided pruning, but the final free energy estimates remain relatively stable, demonstrating the robustness of the network-wide analysis[58,61] even when CC errors are initially large. This does not imply that large CC errors resulting from unconstrained edge free energy analysis can be ignored. Rather, the origins of these errors should be checked, as they often result from alchemical transformation pathways that have poor phase space overlap and are difficult to sample consistently. As illustrated here, sometimes the network-wide free energy analysis with CC constraints is sufficiently robust to produce free energy estimates that are largely invariant to cycle closure errors; however, this cannot generally be relied upon and should be examined. The use of iterative LMI pruning is one way to ascertain the degree to which this is the case.

4.6. Comparison of the Computational Cost of RBFE, CBFE, and ABFE Calculations

Table 1 summarizes the computational cost of CBFE relative to RBFE and ABFE for the TYK2 and BRD4 systems across simulations using 12, 25, and 40 λ windows. For TYK2, we were able to perform all three types of FEP due to the congeneric nature of the ligands and can therefore compare the computational cost across RBFE, CBFE, and ABFE, while for BRD4, where the ligands are noncongeneric and RBFE was not possible, we only compare CBFE and ABFE.

Table 1. Computational Cost (GPU-Hours) for RBFE, CBFE, and ABFE Calculations on the Tyk2 and BRD4 Systems Using Different Numbers of λ Windows[a]

	Number of λ windows		
	12	25	40
	RBFE		
tyk2	3.97	7.68	11.39
brd4	–	–	–
	CBFE		
tyk2	6.22	12.81	18.82
brd4	4.33	8.39	12.09
	ABFE		
tyk2	16.80	35.88	52.18
brd4	9.95	19.82	28.73

[a]For Tyk2, the protein-ligand complex and solvated ligand systems contain ≈31k and ≈6k atoms, respectively; for BRD4, they contain ≈17k and ≈9k atoms. In case of ABFE, the GPU-hours reported are for two ligands, in order to be consistent with RBFE and CBFE calculations. All calculations were run on NVIDIA RTX A4500 GPUs.

In TYK2, an RBFE calculation between two ligands for a typical edge requires just under 4 GPU-hours. Using the same number of λ windows, a CBFE calculation requires slightly more than 6 GPU-hours (≈1.5× RBFE), whereas an ABFE calculation for two ligands requires nearly 17 GPU-hours (>4× RBFE). In practice, however, RBFE calculations typically converge with 12 λ windows, while CBFE and ABFE generally require 25 and 40 λ windows, respectively. Under these more realistic settings, a CBFE calculation for TYK2 takes approximately 12.8 GPU-hours (a little over 3× RBFE), and an ABFE calculation takes roughly 52 GPU-hours (13× RBFE and >3× CBFE). Simulations on the BRD4 system shows a similar pattern: a CBFE calculation with 25 λ windows requires 8.4 GPU-hours, whereas an ABFE calculation with 40 λ windows requires 28.7 GPU-hours (>3× the cost of CBFE). Thus, for calculating relative binding free energies between dissimilar ligands that are beyond the scope of RBFE, CBFE offers considerable efficiency over ABFE.

5. CONCLUSION

In conclusion, we present a new computational methodology, CBFE, that enables the accurate and efficient estimation of relative binding free energies for molecules with dissimilar scaffolds. Traditional RBFE calculations are well established for predicting the potencies of congeneric series with shared scaffolds but are less effective for structurally diverse ligands. By leveraging the alchemical enhanced sampling technique previously demonstrated to improve the precision of RBFE calculations, together with λ-dependent Boresch restraints to eliminate the need for additional simulations, we demonstrate that the CBFE approach provides reliable, computationally tractable free energy estimates for a wide range of ligands for the TYK2, CHK1, BACE1, and BRD4 systems. Future work will focus on further improvements to the efficiency and performance of the method.

■ ASSOCIATED CONTENT

Data Availability Statement

Details of the RBFE, CBFE, and ABFE protocols employed in this study are described in the Methods section and Supporting Information. All methodological developments in this work, including the λ-dependent Boresch restraints, are available in the latest version of AMBER (AMBER24). All files required to reproduce the simulations, including protein and ligand starting structures, AMBER topology files with associated force field parameters, restart files, and relevant AMBER input files (in PDB, SDF, PARM7, RST7, and text formats), as well as the results from all edge and ligand binding free energy calculations, are made available through Zenodo (10.5281/zenodo.17101942).

Supporting Information

The Supporting Information is available free of charge at https://pubs.acs.org/doi/10.1021/acs.jcim.5c02204.

Additional details related to cycle closure error analysis; illustration of Boresch restraints employed in CBFE and ABFE calculations; thermodynamic cycle employed in ABFE calculations; summary of the four data sets considered in this study, including 2D structures and calculated binding free energies of all 56 ligands across the four data sets; summary of cycle closure analysis on all four data sets, including additional cycle closure analysis with iterative LMI pruning on BACE1 and BRD4 data sets (PDF)

The SI Zip file contains all tex files and figures that are necessary to generate the SI PDF file (ZIP)

■ AUTHOR INFORMATION

Corresponding Authors

Darrin M. York − *Laboratory for Biomolecular Simulation Research,Institute for Quantitative Biomedicine and Department of Chemistry and Chemical Biology, Rutgers University, Piscataway, New Jersey 08854, United States;* orcid.org/0000-0002-9193-7055; Email: Darrin.York@rutgers.edu

https://doi.org/10.1021/acs.jcim.5c02204
J. Chem. Inf. Model. 2026, 66, 1626−1636

Abir Ganguly − *TandemAI, New York, New York 10036, United States;* orcid.org/0000-0002-0630-1109; Email: abir.ganguly@tandemai.com
Albert C. Pan − *TandemAI, New York, New York 10036, United States*; Email: albert.pan@tandemai.com

Authors

Hsu-Chun Tsai − *TandemAI, New York, New York 10036, United States;* orcid.org/0000-0001-7027-5649
Shi Zhang − *Laboratory for Biomolecular Simulation Research,Institute for Quantitative Biomedicine and Department of Chemistry and Chemical Biology, Rutgers University, Piscataway, New Jersey 08854, United States*
Tai-Sung Lee − *Laboratory for Biomolecular Simulation Research,Institute for Quantitative Biomedicine and Department of Chemistry and Chemical Biology, Rutgers University, Piscataway, New Jersey 08854, United States;* orcid.org/0000-0003-2110-2279
Timothy J. Giese − *Laboratory for Biomolecular Simulation Research,Institute for Quantitative Biomedicine and Department of Chemistry and Chemical Biology, Rutgers University, Piscataway, New Jersey 08854, United States*
Charles Lin − *TandemAI, New York, New York 10036, United States*
James Xu − *TandemAI, New York, New York 10036, United States*
Yinhui Yi − *TandemAI, New York, New York 10036, United States*

Complete contact information is available at: https://pubs.acs.org/10.1021/acs.jcim.5c02204

Author Contributions

H.-C.T. performed the calculations. S.Z. conducted the network-wide free energy analysis. T.-S.L. and T.J.G. contributed to the implementation of lambda-dependent restraints in AMBER and to the cycle closure analysis, respectively. C.L., J.X., and Y.Y. contributed to the implementation of the CBFE protocol. D.M.Y., A.G., and A.C.P. conceived the project, designed the research, and supervised the study. H.-C.T., D.M.Y., A.G., and A.C.P. wrote the original draft of the manuscript. All authors reviewed and approved the final version of the manuscript.

Notes

The authors declare no competing financial interest.

■ ACKNOWLEDGMENTS

The authors are grateful for the financial support provided by the National Institutes of Health (No. GM107485 to D.M.Y., GM149874 to T.L.). Computational resources were provided by the Office of Advanced Research Computing (OARC) at Rutgers, The State University of New Jersey; the Advanced Cyberinfrastructure Coordination Ecosystem: Services & Support (ACCESS) program, which is supported by the National Science Foundation (supercomputer Expanse at SDSC through allocation CHE190067); the Texas Advanced Computing Center (TACC) at the University of Texas at Austin (supercomputer Frontera through allocation CHE20002); and the INCITE program through the Argonne Leadership Computing Facility at Argonne National Laboratory, which is supported by the Office of Science of the U.S. DOE under Contract No. DEAC02-06CH11357 (supercomputer Polaris through INCITE allocation 13127). We also thank Rae Qi, Kenneth Lam, and Thomas Watson for helpful discussions.

■ REFERENCES

(1) York, D. M. Modern Alchemical Free Energy Methods for Drug Discovery Explained. *ACS Phys.Chem. Au.* **2023**, *3*, 478−491.
(2) Cournia, Z.; Chipot, C.; Roux, B.; York, D. M.; Sherman, W. Free Energy Methods in Drug DiscoveryâIntroduction. *ACS Symp. Ser.* **2021**, *1397*, 1−38.
(3) King, E.; Aitchison, E.; Li, H.; Luo, R. Recent Developments in Free Energy Calculations for Drug Discovery. *Front. Mol. Biosci.* **2021**, *8*, 712085.
(4) He, X.; Liu, S.; Lee, T.-S.; Ji, B.; Man, V. H.; York, D. M.; Wang, J. Fast, Accurate, and Reliable Protocols for Routine Calculations of Protein-Ligand Binding Affinities in Drug Design Projects Using AMBER GPU-TI with ff14SB/GAFF. *ACS Omega* **2020**, *5*, 4611−4619.
(5) Adediwura, V. A.; Koirala, K.; Do, H. N.; Wang, J.; Miao, Y. Understanding the impact of binding free energy and kinetics calculations in modern drug discovery. *Expert Opin. Drug Discovery* **2024**, *19*, 671−682.
(6) Wang, L.; Wu, Y.; Deng, Y.; Kim, B.; Pierce, L.; Krilov, G.; Lupyan, D.; Robinson, S.; Dahlgren, M. K.; Greenwood, J.; et al. Accurate and Reliable Prediction of Relative Ligand Binding Potency in Prospective Drug Discovery by Way of a Modern Free-Energy Calculation Protocol and Force Field. *J. Am. Chem. Soc.* **2015**, *137*, 2695−2703.
(7) Lee, T.-S.; Lin, Z.; Allen, B. K.; Lin, C.; Radak, B. K.; Tao, Y.; Tsai, H.-C.; Sherman, W.; York, D. M. Improved Alchemical Free Energy Calculations with Optimized Smoothstep Softcore Potentials. *J. Chem. Theory Comput.* **2020**, *16*, 5512−5525.
(8) Ganguly, A.; Tsai, H.-C.; Fernández-Pendás, M.; Lee, T.-S.; Giese, T. J.; York, D. M. AMBER Drug Discovery Boost Tools: Automated Workflow for Production Free-Energy Simulation Setup and Analysis (ProFESSA). *J. Chem. Inf. Model* **2022**, *62*, 6069−6083.
(9) Boresch, S. B.; Tettinger, F.; Leitgeb, M.; Karplus, M. Absolute Binding Free Energies: A Quantitative Approach for Their Calculation. *J. Phys. Chem. B* **2003**, *107*, 9535−9551.
(10) Boresch, S. On Analytical Corrections for Restraints in Absolute Binding Free Energy Calculations. *J. Chem. Inf. Model* **2024**, *64*, 3605−3609.
(11) Wu, Z.; Konig, G.; Boresch, S.; Cossins, B. P. Optimizing Absolute Binding Free Energy Calculations for Production Usage ASAP. *J. Chem. Theory Comput.* **2025**, *21*, 8330−8340.
(12) Lee, T.-S. L.; Tsai, H.-C.; Ganguly, A.; York, D. M. ACES: Optimized Alchemically Enhanced Sampling. *J. Chem. Theory Comput.* **2023**, *19*, 472−487.
(13) Tsai, H.-C.; Xu, J.; Guo, Z.; Yi, Y.; Tian, C.; Que, X.; Giese Timothy Lee, T.-S.; Lee, T.-S.; York, D. M.; Ganguly, A.; et al. Improvements in Precision of Relative Binding Free Energy Calculations Afforded by the Alchemical Enhanced Sampling (ACES) Approach. *J. Chem. Inf. Model* **2024**, *64*, 7046−7055.
(14) Zhang, S.; Giese, T. J.; Lee, T.-S.; York, D. M. Alchemical Enhanced Sampling with Optimized Phase Space Overlap. *J. Chem. Theory Comput.* **2024**, *20*, 3935−3953.
(15) Lee, T.-S.; Cerutti, D. S.; Mermelstein, D.; Lin, C.; Le Grand, S.; Giese, T. J.; Roitberg, A.; Case, D. A.; Walker, R. C.; York, D. M. GPU-Accelerated Molecular Dynamics and Free Energy Methods in Amber18: Performance Enhancements and New Features. *J. Chem. Inf. Model* **2018**, *58*, 2043−2050.
(16) Giese, T. J.; York, D. M. A GPU-Accelerated Parameter Interpolation Thermodynamic Integration Free Energy Method. *J. Chem. Theory Comput.* **2018**, *14*, 1564−1582.
(17) Lee, T.-S.; Hu, Y.; Sherborne, B.; Guo, Z.; York, D. M. Toward Fast and Accurate Binding Affinity Prediction with pmemdGTI: An Efficient Implementation of GPU-Accelerated Thermodynamic Integration. *J. Chem. Theory Comput.* **2017**, *13*, 3077−3084.

(18) Okamoto, Y. Generalized-ensemble algorithms: Enhanced sampling techniques for Monte Carlo and molecular dynamics simulations. *J. Mol. Graph. Model* **2004**, *22*, 425−439.
(19) Hritz, J.; Oostenbrink, C. Hamiltonian Replica Exchange Molecular Dynamics Using Soft-core Interactions. *J. Chem. Phys.* **2008**, *128*, 144121.
(20) Tsai, H.-C.; Lee, T.-S.; Ganguly, A.; Giese, T. J.; Ebert, M. C.; Labute, P.; Merz, K. M. J.; York, D. M. AMBER Free Energy Tools: A New Framework for the Design of Optimized Alchemical Transformation Pathways. *J. Chem. Theory Comput.* **2023**, *19*, 640−658.
(21) Clark, F.; Robb, G. R.; Cole, D. J.; Michel, J. Automated Adaptive Absolute Binding Free Energy Calculations. *J. Chem. Theory Comput.* **2024**, *20*, 7806−7828.
(22) Ghahremanpour, M. M.; Saar, A.; Tirado-Rives, J.; Jorgensen, W. L. Computation of Absolute Binding Free Energies for Noncovalent Inhibitors with SARS-CoV-2 Main Protease. *J. Chem. Inf. Model* **2023**, *63*, 5309−5318.
(23) Qian, Y.; Cabeza de Vaca, I.; Vilseck, J. Z.; Cole, D. J.; Tirado-Rives, J.; Jorgensen, W. L. Absolute Free Energy of Binding Calculations for Macrophage Migration Inhibitory Factor in Complex with a Druglike Inhibitor. *J. Phys. Chem. B* **2019**, *123*, 8675−8685.
(24) Li, P.; Pu, T.; Mei, Y. FEP-SPell-ABFE: An OpenSource Automated Alchemical Absolute Binding Free-Energy Calculation Workflow for Drug Discovery. *J. Chem. Inf. Model* **2025**, *65*, 2711−2721.
(25) Pal, R. K.; Gallicchio, E. Perturbation potentials to overcome order/disorder transitions in alchemical binding free energy calculations. *J. Chem. Phys.* **2019**, *151*, 124116.
(26) Khuttan, S.; Azimi, S.; Wu, J. Z.; Gallicchio, E. Alchemical transformations for concerted hydration free energy estimation with explicit solvation. *J. Chem. Phys.* **2021**, *154*, 054103.
(27) Wu, J. Z.; Azimi, S.; Khuttan, S.; Deng, N.; Gallic-Chio, E. Alchemical Transfer Approach to Absolute Binding Free Energy Estimation. *J. Chem. Theory Comput.* **2021**, *17*, 3309−3319.
(28) Sabanés Zariquiey, F.; Pérez, A.; Majewski, M.; Gallicchio, E.; De Fabritiis, G. Validation of the Alchemical Transfer Method for the Estimation of Relative Binding Affinities of Molecular Series. *J. Chem. Inf. Model* **2023**, *63*, 2438−2444.
(29) Baumann, H. M.; Dybeck, E.; McClendon, C. L.; Pickard, F. C. I.; Gapsys, V.; Pérez-Benito, L.; Hahn, D. F.; Tresadern, G.; Mathiowetz, A. M.; Mobley, D. L. Broadening the Scope of Binding Free Energy Calculations Using a Separated Topologies Approach. *J. Chem. Theory Comput.* **2023**, *19*, 5058−5076.
(30) Rocklin, G. J.; Mobley, D. L.; Dill, K. A. Separated topologies—A method for relative binding free energy calculations using orientational restraints. *J. Chem. Phys.* **2013**, *138*, 085104.
(31) Wang, L.; Deng, Y.; Wu, Y.; Kim, B.; Le Bard, D. N.; Wandschneider, D.; Beachy, M.; Friesner, R. A.; Abel, R. Accurate Modeling of Scaffold Hopping Transformations in Drug Discovery. *J. Chem.Theory Comput.* **2017**, *13*, 42−54.
(32) Procacci, P. Relative Binding Free Energy between Chemically Distant Compounds Using a Bidirectional Nonequilibrium Approach. *J. Chem. Theory Comput.* **2022**, *18*, 4014−4026.
(33) Ries, B.; Normak, K.; Weiß, R. G.; Rieder, S.; Barros, E. P.; Champion, C.; König, G.; Riniker, S. Relative free-energy calculations for scaffold hopping-type transformations with an automated RE-EDS sampling procedure. *J. Comput. Aided Mol. Des.* **2022**, *36*, 117−130.
(34) Zou, J.; Li, Z.; Liu, S.; Peng, C.; Fang, D.; Wan, X.; Lin, Z.; Lee, T.-S.; Raleigh, D. P.; Yang, M.; Simmerling, C. Scaffold Hopping Transformations Using Auxiliary Restraints for Calculating Accurate Relative Binding Free Energies. *J. Chem. Theory Comput.* **2021**, *17*, 3710−3726.
(35) Lee, T.-S.; Allen, B. K.; Giese, T. J.; Guo, Z.; Li, P.; Lin, C.; McGee, T. D. J.; Pearlman, D. A.; Radak, B. K.; Tao, Y.; Tsai, H.-C.; Xu, H.; Sherman, W.; York, D. M. Alchemical Binding Free Energy Calculations in AMBER20: Advances and Best Practices for Drug Discovery. *J. Chem. Inf. Model* **2020**, *60*, 5595−5623.
(36) Huang, X.; Cheng, C. C.; Fischmann, T. O.; Duca, J. S.; Yang, X.; Richards, M.; Shipps, G. W. J. Discovery of a Novel Series of CHK1 Kinase Inhibitors with a Distinctive Hinge Binding Mode. *ACS Med. Chem. Lett.* **2012**, *3*, 123−128.
(37) Malamas, M. S.; Barnes, K.; Johnson, M.; Hui, Y.; Zhou, P.; Turner, J.; Hu, Y.; Wagner, E.; Fan, K.; Chopra, R.; Olland, A.; Bard, J.; Pangalos, M.; Reinhart, P.; Robichaud, A. J. Di-substituted pyridinyl aminohydantoins as potent and highly selective human β-secretase (BACE1) inhibitors. *Bioorg. Med. Chem.* **2010**, *18*, 630−639.
(38) Hunt, K. W.; Cook, A. W.; Watts, R. J.; Clark, C. T.; Vigers, G.; Smith, D.; Metcalf, A. T.; Gunawardana, I. W.; Burkard, M.; Cox, A. A.; et al. Spirocyclic β-Site Amyloid Precursor Protein Cleaving Enzyme 1 (BACE1) Inhibitors: From Hit to Lowering of Cerebrospinal Fluid (CSF) Amy loid β in a Higher Species. *J. Med. Chem.* **2013**, *56*, 3379−3403.
(39) Oehlrich, D.; Peschiulli, A.; Tresadern, G.; Van Gool, M.; Antonio Vega, J.; De Lucas, A. I.; Alonso de Diego, S. A.; Prokopcova, H.; Austin, N.; Van Brandt, S.; et al. Evaluation of a Series of β-Secretase 1 Inhibitors Containing Novel Heteroaryl-Fused-Piperazine Amidine Warheads. *ACS Med. Chem. Lett.* **2019**, *10*, 1159−1165.
(40) Lin, Z.; Zou, J.; Liu, S.; Peng, C.; Li, Z.; Wan, X.; Fang, D.; Yin, J.; Gobbo, G.; Chen, Y.; Ma, J.; Wen, S.; Zhang, P.; Yang, M. A Cloud Computing Platform for Scalable Relative and Absolute Binding Free Energy Predictions: New Opportunities and Challenges for Drug Discovery. *J. Chem. Inf. Model* **2021**, *61*, 2720−2732.
(41) Lin, Z.; Zou, J.; Liu, S.; Peng, C.; Li, Z.; Wan, X.; Fang, D.; Yin, J.; Gobbo, G.; Chen, Y.; Ma, J.; Wen, S.; Zhang, P.; Yang, M. Correction to "A Cloud Computing Platform for Scalable Relative and Absolute Binding Free Energy Prediction: New Opportunities and Challenges for Drug Discovery". *J. Chem. Inf. Model* **2021**, *61*, 4819.
(42) Case, D. A.; Aktulga, H. M.; Belfon, K.; Cerutti, D. S.; Cisneros, G. A.; Cruzeiro, V. W. D.; Forouzesh, N.; Giese, T. J.; Gotz, A. W.; Gohlke, H.; et al. AmberTools. *J. Chem. Inf. Model* **2023**, *63*, 6183−6191.
(43) Jorgensen, W. L.; Chandrasekhar, J.; Madura, J. D.; Impey, R. W.; Klein, M. L. Comparison of Simple Potential Functions for Simulating Liquid Water. *J. Chem. Phys.* **1983**, *79*, 926−935.
(44) Maier, J. A.; Martinez, C.; Kasavajhala, K.; Wickstrom, L.; Hauser, K. E.; Simmerling, C. ff14SB: Improving the Accuracy of Protein Side Chain and Backbone Parameters from ff99SB. *J. Chem. Theory Comput.* **2015**, *11*, 3696−3713.
(45) Wang, J.; Wolf, R. M.; Caldwell, J. W.; Kollman, P. A.; Case, D. A. Development and testing of a general amber force field. *J. Comput. Chem.* **2004**, *25*, 1157−1174.
(46) Jakalian, A.; Bush, B. L.; Jack, D. B.; Bayly, C. I. Fast, efficient generation of high-quality atomic charges. AM1-BCC model: I. *Method. J. Comput. Chem.* **2000**, *21*, 132−146.
(47) Hoover, W. G.; Ree, F. H. Use of Computer Experiments to Locate the Melting Transition and Calculate the Entropy in the Solid Phase. *J. Chem. Phys.* **1967**, *47*, 4873−4878.
(48) Miyamoto, S.; Kollman, P. A. SETTLE: An Analytical Version of the SHAKE and RATTLE Algorithm for Rigid Water Models. *J. Comput. Chem.* **1992**, *13*, 952−962.
(49) Ryckaert, J. P.; Ciccotti, G.; Berendsen, H. J. C. Numerical Integration of the Cartesian Equations of Motion of a System with Constraints: Molecular Dynamics of n-alkanes. *J. Comput. Phys.* **1977**, *23*, 327−341.
(50) Hopkins, C. W.; Le Grand, S.; Walker, R. C.; Roit Berg, A. E. Long-Time-Step Molecular Dynamics through Hydrogen Mass Repartitioning. *J. Chem. Theory Comput.* **2015**, *11*, 1864−1874.
(51) Darden, T.; York, D.; Pedersen, L. Particle Mesh Ewald: An N·log(N) Method for Ewald Sums in Large Systems. *J. Chem. Phys.* **1993**, *98*, 10089−10092.
(52) Essmann, U.; Perera, L.; Berkowitz, M. L.; Darden, T.; Lee, H.; Pedersen, L. G. A Smooth Particle Mesh Ewald Method. *J. Chem. Phys.* **1995**, *103*, 8577−8593.
(53) Case, D.; Aktulga, H.; Belfon, K.; Ben-Shalom, I.; Berryman, J.; Brozell, S.; Carvahol, F.; Cerutti, D.; Cheatham, T., III; Cisneros, G., et al. *AMBER 2025*; University of California: San Francisco, CA, 2025.

https://doi.org/10.1021/acs.jcim.5c02204
J. Chem. Inf. Model. 2026, 66, 1626−1636

(54) Case, D. A.; Cerutti, D. S.; Cruzeiro, V. W. D.; Darden, T. A.; Duke, R. E.; Ghazimirsaeed, M.; Giambasu, G. M.; Giese, T. J.; Götz, A. W.; Harris, J. A.; et al. Recent Developments in Amber Biomolecular Simulations. *J. Chem. Inf. Model* **2025**, *65*, 7835−7843.
(55) Tsai, H.-C.; Tao, Y.; Lee, T.-S.; Merz, K. M.; York, D. M. Validation of Free Energy Methods in AMBER. *J. Chem. Inf. Model* **2020**, *60*, 5296−5300.
(56) Huggins, D. J. Comparing the Performance of Different AMBER Protein Forcefields, Partial Charge Assignments, and Water Models for Absolute Binding Free Energy Calculations. *J. Chem. Theory Comput.* **2022**, *18*, 2616−2630.
(57) Alibay, I.; Magarkar, A.; Seeliger, D.; Biggin, P. C. Evaluating the use of absolute binding free energy in the fragment optimisation process. *Commun. Chem.* **2022**, *5*, 105.
(58) Giese, T. J.; Snyder, R.; Piskulich, Z.; Barletta, G. P.; Zhang, S.; McCarthy, E.; Ekesan, S.; York, D. M. FE-ToolKit: A Versatile Software Suite for Analysis of High- Dimensional Free Energy Surfaces and Alchemical Free Energy Networks. *J. Chem. Inf. Model* **2025**, *65*, 5273−5279.
(59) Case, D. A.; Cerutti, D. S.; Cruzeiro, V. W. D.; Darden, T. A.; Duke, R. E.; Ghazimirsaeed, M.; Giambasu, G. M.; Giese, T. J.; Götz, A. W.; Harris, J. A.; et al. Recent Developments in Amber Biomolecular Simulations. *J. Chem. Inf. Model* **2025**, *65*, 7835−7843.
(60) Shirts, M. R.; Chodera, J. D. Statistically optimal analysis of samples from multiple equilibrium states. *J. Chem. Phys.* **2008**, *129*, 124105.
(61) Giese, T. J.; York, D. M. Variational Method for Networkwide Analysis of Relative Ligand Binding Free Energies with Loop Closure and Experimental Constraints. *J. Chem. Theory Comput.* **2021**, *17*, 1326−1336.
(62) Aldeghi, M.; Heifetz, A.; Bodkin, M. J.; Knapp, S.; Biggin, P. C. Accurate calculation of the absolute free energy of binding for drug molecules. *Chem. Sci.* **2016**, *7*, 207−218.

https://doi.org/10.1021/acs.jcim.5c02204
J. Chem. Inf. Model. 2026, 66, 1626−1636